Protective Iron Carbonate Films—Part 2: Chemical Removal by Dissolution in Single-Phase Aqueous Flow

V. Ruzic,‡, M. Veidt,* and S. Nešić***

ABSTRACT

The dissolution of deposited, protective iron carbonate films in oil and gas transportation pipelines may drastically enhance corrosive processes on steel surfaces, and thus, seriously affect the longevity of the equipment in use. An investigation had been carried out to get a better understanding of the kinetics and underlying mechanism of film dissolution, as well as to provide baseline data for further study of the possible synergistic effect between chemical and mechanical film removal. To address this goal, a series of iron carbonate film dissolution experiments was conducted covering a wide range of pH values (pH 3 to pH 6.1) and Reynolds numbers ($Re = 3.68 \times 10^3$ to 1.84×10^5) using a rotating cylinder configuration. The polarization resistance technique was used for implicit quantification of film removal kinetics via corrosion rate monitoring, whereas scanning electron microscopy was utilized for the purpose of residual film characterization. The results suggested that chemical film dissolution was governed by mass transfer and showed the strong dependence of film removal kinetics on the level of saturation in the solution (pH value) and fluid velocity. In addition, the physical mechanism of chemical film removal has been explained and discussed in light of the obtained results.

KEY WORDS: carbon dioxide corrosion, film dissolution, mass-transfer control, protective iron carbonate film, rotating cylinder electrode, turbulent single-phase flow

INTRODUCTION

Iron carbonate ($FeCO_3$) films formed on mild steel equipment, encountered in the oil and gas production and transportation industry, generally provide satisfactory protection from potentially destructive acts of internal pipeline corrosion.[1-2] It is commonly known that they can be damaged chemically by dissolution and/or mechanically by hydrodynamic forces. While the mechanical removal of $FeCO_3$ scales has been previously reported by Ruzic, et al.,[3] virtually no information is available in the open literature on the dissolution of these films.

The $FeCO_3$ dissolution/precipitation reaction can be written as:

$$FeCO_3(s) \Leftrightarrow Fe^{2+} + CO_3^{2-} \quad (1)$$

When the forward rate is equal to the backward rate, the $FeCO_3$ film is in equilibrium with the species in solution. Hence, supersaturation (S) is defined as:

$$S = \frac{[Fe^{2+}][CO_3^{2-}]}{K_{sp}} \quad (2)$$

where [ ] denotes concentration of the species and K_{sp} is the solubility product (equilibrium constant). For equilibrium (saturation), S = 1. It is known that the

Submitted for publication June 2005; in revised form, December 2005. Part 1 of this manuscript appears in *Corrosion* 62, 5 (2006), p. 419-432.

‡ Corresponding author. E-mail: v.ruzic@uq.edu.au.
* Department of Mechanical Engineering, The University of Queensland, Brisbane Queensland 4072, Australia.
** Institute for Corrosion and Multiphase Flow Technology, Chemical Engineering Department, Ohio University, 340 ½ W. State St., Stocker Center, Athens, OH 45701.

0010-9312/06/000115/$5.00+$0.50/0

protective layer can be readily dissolved when exposed to an undersaturated solution (S < 1). Considering that pH values found in oil and gas production waters typically vary between pH 4 and pH 6,[4] favorable conditions for dissolution are relatively easily satisfied in practice at the lower pH range.

The dissolution process is believed to be governed by mass transfer.[5-6] The key argument often quoted as supportive of the hypothesized mass-transfer-controlled dissolution is absent/diminished increase in flow dependence with increased temperature[6-7] or decreased pH value.[8] For example, according to Crocker, et al.,[8] a diminished increase in removal rate with an increasing Reynolds number exhibited at lower pH served as a valid confirmation of the mass-transfer-limiting mechanism playing the key role in the film removal process. Several attempts have been made to numerically predict dissolution rates assuming mass-transfer-based models and verify them with limited experimental data.[9-10] It has been found that dissolution produces a roughening of crystalline surfaces under flowing conditions;[9,11-12] however, contradictory results obtained in stagnant situations have been reported. For example, Wolynec and Gabe[11] documented augmented surface irregularity as opposed to Crouch and Ryan,[13] who reported general surface smoothening attributed to the removal of superficial asperities. The only previous study that took a comprehensive approach toward the film removal process was the one by Giralt and Trass.[12] A model-material (trans-cinnamic acid) was used in this work, in which the authors successfully pointed out the importance of interactions between chemical and mechanical effects of flow. Silverman has shown the relationship between the wall shear stress and mass-transfer rates.[14] Although his work did not deal with film dissolution per se, it implies that chemical removal, as well as mechanical, is related to hydrodynamic parameters. A small number of studies dealt with other types of corrosion products such as thin passive films,[10,13] while others looked at cases unrelated to corrosion such as the dissolution of calcium carbonate scales, i.e., calcite ($CaCO_3$)[8-9] as well as various model materials.[12]

The lack of pure chemical dissolution baseline data that would enable the identification of any synergistic effects between the two film removal mechanisms (dissolution and mechanical removal) was the primary motivation for this study. Hence, the present work reports on experimental investigations of $FeCO_3$ film dissolution in carbon dioxide (CO_2) corrosive environments. It covers the chemical film removal kinetics and film damage characterization in undisturbed single-phase turbulent flow. This is a follow-up to the pure mechanical $FeCO_3$ film removal study by Ruzic, et al.[3]

EXPERIMENTAL PROCEDURES

The three-electrode rotating cylinder (RC) setup was used to perform the film dissolution experiments. The cylindrical specimens, outer diameter (OD) 12 mm by 10 mm, were fabricated from 1020 mild steel. A saturated silver/silver chloride (Ag/AgCl) electrode and platinum wire served as a reference (RE) and counter electrode (CE), respectively. The solution was made up of CO_2-purged distilled water and 1 wt% sodium chloride (NaCl). All samples were polished with 1000-grit sandpaper and properly degreased, cleaned, and processed before submersion. The operating conditions were atmospheric pressure (101 kPa) and 80°C temperature at which the partial pressure of CO_2 gaseous phase was p_{CO_2} = 0.54 bar.

The corrosion rates (CR) were monitored by using the linear polarization resistance (LPR) electrochemical measurement technique. The thickness and morphology of the film were assessed using scanning electron microscopy (SEM). In addition, the energy-dispersive spectroscopy (EDS) and x-ray mapping (XRM) elemental compositional analysis of the corrosion products were carried out. The latter, although only qualitative, provides elemental analysis over a much wider area, and is capable of performing phase analysis.

Film Formation Procedure

$FeCO_3$ films were formed in-situ by precipitation in a chemically controlled aqueous environment at 200 rpm rotational speed (v = 0.13 m/s specimen peripheral velocity; Re = 3.68×10^3). An external glass column packed with fine steel wool maintained an additional source of ferrous ion (Fe^{2+}) supply to the main cell. The pH was increased to 6.9 by adding sodium hydrogen carbonate ($NaHCO_3$). The specimen was then subjected to a 4-hour, forced precorrosion period at 10 μm/h rate. This procedure led to the formation of very protective and thick layers (CR < 0.05 mm/y and δ ≈ 50 μm) with smooth and uniform surfaces in approximately 2 days. More on the film growth methodology,[(1)] as well as on the utilized equipment, solution chemical composition, and specimen and solution preparation procedures, can be found in Ruzic, et al.[3]

Film Dissolution Procedure

Once a very protective film had formed (CR ≤ 0.05 mm/y), the source of additional Fe^{2+} ions was discontinued by shutting off the supply line. This was followed by an increase in rotational speed and a decrease in pH in order to investigate the effect of velocity on film dissolution. The focus was on two rotational speeds in particular: 7,000 rpm (v = 4.40 m/s; Re = 1.29×10^5) and 10,000 rpm (v = 6.28 m/s; Re = 1.84×10^5), as they allowed direct comparison with available pure mechanical film removal data.[3] The film dissolution experiments were conducted over

[(1)] This film growth method was referred to as type B formation procedure in Ruzic, et al.[3]

TABLE 1
Summary of Main Film Dissolution Results[A]

pH	Rotational Speed (rpm)	Final (cut-off) CR (mm/y)	CR gradient (CR_{grad}) (mm/y/h)	Linear CR Range (h)
3	200	3.30	2.6495	0.5 to 0.9
5.5	10,000	0.93	0.3365	0.5 to 1.4
5.55	10,000	0.61 ± 0.04	0.2288 ± 0.0147	0.5 to 1.9 and 0.5 to 2.5
5.6	10,000	0.51 ± 0.00	0.1970 ± 0.0095	0.5 to 2.5
5.7	10,000	0.36 ± 0.00	0.1413 ± 0.0095	0.5 to 2.3
5.8	10,000	0.31 ± 0.01	0.1260 ± 0.0008	0.5 to 2.0
5.8	7,000	0.18 ± 0.01	0.0430 ± 0.0016	0.5 to 2.5
6.1	10,000	0.19 ± 0.01	0.0693 ± 0.0129	0.5 to 1.6

[A] Experimental uncertainties represent standard deviation of the mean, i.e., standard error.

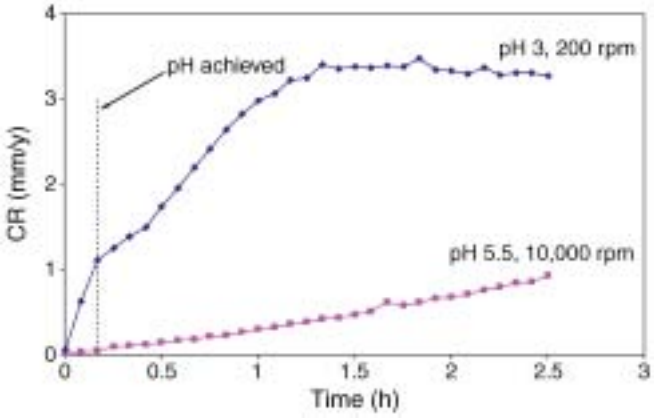

FIGURE 1. *CR increase during film dissolution at: low-pH – low-velocity (pH 3 – 200 rpm) and high-pH – high-velocity (pH 5.5 – 10,000 rpm) combinations.*

a short duration (2.5 h) to avoid mechanical film removal (which is known to have an "initiation" period and typically sets in after 3 h at higher velocity).[3] The dissolution was triggered by converting the water chemistry from a supersaturated to an unsaturated solution via decreasing the pH by adding hydrochloric acid (HCl). This increased the concentration of chloride ions [Cl^-] by up to 10%, which was not considered significant. The desired pH value was adjusted over a 10-min period to enable uniform dilution and mixing of the added HCl with the aqueous media. The concentration of Fe^{2+} ions in bulk solution $[Fe^{2+}]_b$ was followed by phenanthroline calorimetric method. The samples were taken at 0 h (velocity increase point), 0.17 h (after pH adjustment), 1.33 h (midway between pH adjustment and end of experiment), and 2.5 h (end of experiment). The film dissolution rate (in mol/m^2s) is difficult to measure directly and was therefore followed implicitly via CR monitoring. As the protective films dissolved, the CR increased. While this is an indirect technique for measuring the rate of film dissolution, it does follow the key parameter, which is the ultimate goal of this study, and that is the CR. LPR scans during the dissolution phase were repeated every 5 min by polarizing the specimen ±20 mV with a fast scan rate (0.5 mV/s).[2] At the end of the experiment, the specimens were removed from the solutions, flushed with alcohol to dehydrate them, dried, mounted in low viscosity epoxy, and prepared for cross-sectional and topographic SEM examination.

[2] This was four times faster compared to the film formation LPR scan rate.

EXPERIMENTAL RESULTS

The summary of the main film dissolution results discussed in the following sections is given in Table 1.

Effect of pH

Introductory Experiments — In order to get a good starting point, introductory film dissolution experiments with two different pH – velocity combinations were carried out:

—a low-pH (pH 3) – low-velocity (200 rpm) experiment,
—a high-pH (pH 5.5) – high-velocity (10,000 rpm) experiment.

It should be noted that low-dissolution velocity (200 rpm) was exactly the same as film formation velocity. A significant difference in the film removal kinetics was obtained (Figure 1). The low-pH – low-velocity experiment experienced steep CR rise with a plateau (CR = 3.3 mm/y) at 1.3 h. The high-pH – high-velocity experiment led to a much lower CR increase and did not show the plateau. In both cases the "final" corrosion rates can be considered very high and indicate severe damage to the protective film.

SEM inspection of the damaged films showed a striking difference in film appearance between the two cases (Figures 2 and 3), which was consistent with electrochemical CR measurement results (Figure 1). The cross-sectional micrograph (Figure 2[a]) from the low-pH – low-velocity experiment reveals that the specimen was virtually film-free except for some scaly film flakes. The topographic image (Figure 3[a]) shows the flaky film with bare metal directly "visible" through the porous structure. Such film was obvi-

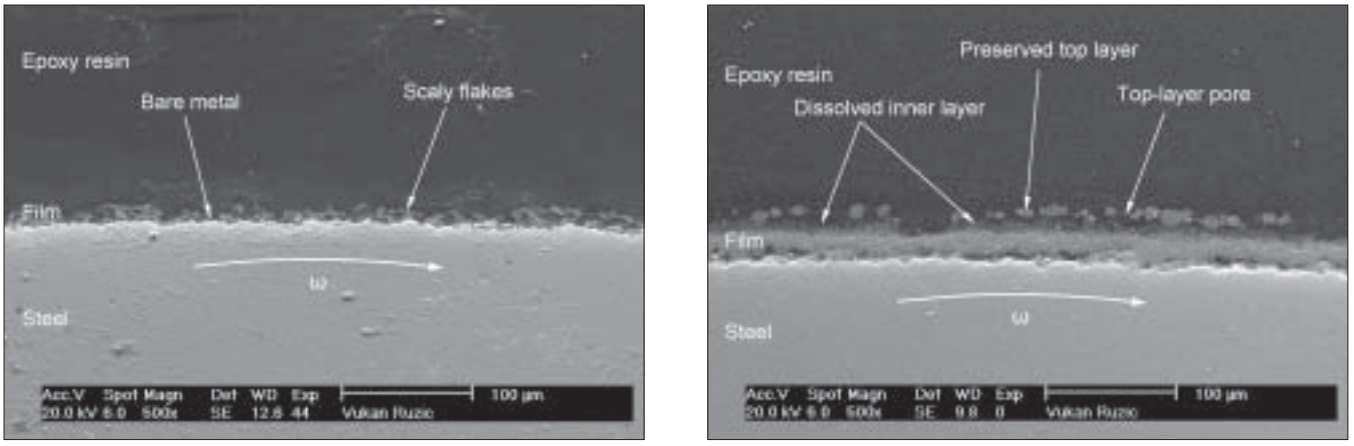

(a) (b)

FIGURE 2. *Typical cross section of: (a) low-pH – low-velocity (pH 3 – 200 rpm) and (b) high-pH – high-velocity (pH 5.5 – 10,000 rpm) $FeCO_3$ film residual at the end of dissolution process (mag. 500X).*

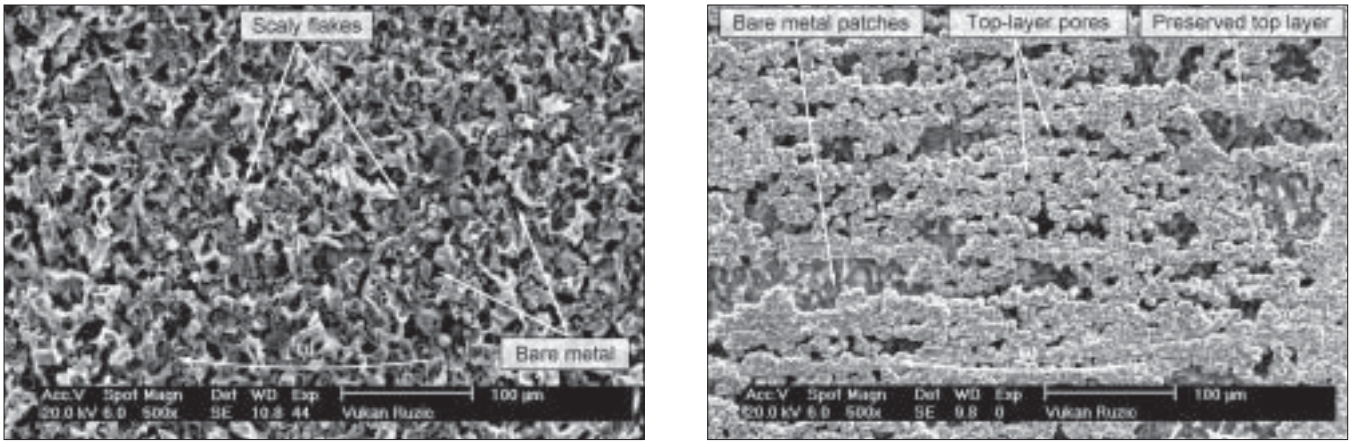

(a) (b)

FIGURE 3. *Typical surface topography of: (a) low-pH – low-velocity (pH 3 – 200 rpm) and (b) high-pH – high-velocity (pH 5.5 – 10,000 rpm) $FeCO_3$ film residual at the end of dissolution process (mag. 500X).*

ously not capable of providing any corrosion protection to the parent material.

In contrast, the overall structure of high-pH – high-velocity damaged film was generally well preserved. The film dissolution was only partial because of the higher pH value. Nevertheless, quite serious damage did take place at certain localities on the film (Figures 2[b] and 3[b]), which can explain the relatively high final CR seen in Figure 1. The cross-sectional area exhibits a "notched" film appearance with significant film dissolution occurring just underneath the top film layer (Figure 2[b]). This interesting observation will be discussed in detail below. The film surface topographic image shows both the intact crystal grains at the top film layer as well as bare metal patches in some locations (Figure 3[b]). EDS compositional analysis and x-ray mapping (XRM) verified these visual observations.

Several important conclusions have been drawn from this set of introductory experiments, which directed further experimental design. The low pH dissolution process, even at low velocity, has been found unsatisfactory, as nearly complete film removal occurred in a short period, not leaving the opportunity for detailed damage characterization. The high-pH case yielded partially damaged films with no signs of primary, macroscopic mechanical film removal (mode M) previously observed in Ruzic, et al.,[3] and was selected for further studies.

However, the origin of occasional microscopic bare patches that were oriented in the flow direction (Figure 3[b]) remains puzzling. It can only be speculated that they evolved from pure and selective chemical dissolution of the film (mode D), although the effect of mechanical film removal induced by dissolution (mode M/D) cannot be ruled out completely.

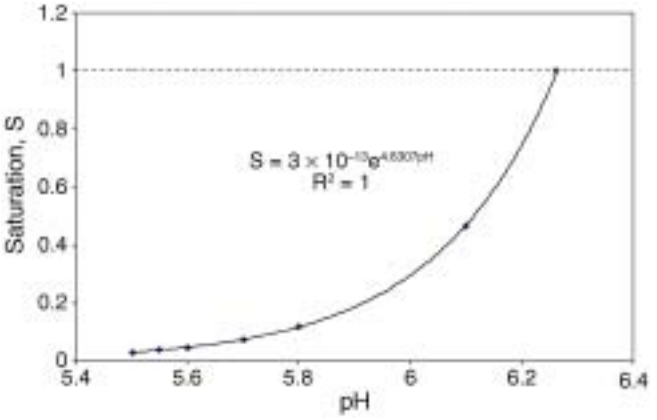

FIGURE 4. *Predicted (under)saturation (S), computed for given pH and measured bulk Fe^{2+} concentration $[Fe^{2+}]_b$ at the beginning of chemical film removal process (t = 0 h) for 80°C.*

It has been suggested by Giralt and Trass[12] that a synergistic action may occur between the two forms of crystal grain removal once the critical shear stress exceeds threshold values. Therefore, the following experimental series focused on establishing that the damage was caused solely by film dissolution.

Dissolution Kinetics Experiments — In this series of experiments pH was varied in the range from 5.5 to 6.1. Corresponding calculated (under)saturations, based on mean measured $[Fe^{2+}]_b$ at 0 h, varied from S = 0.03 to S = 0.46 (Figure 4).

In all experiments conducted at 10,000 rpm the inception of the dissolution process was instantaneous, reaching the local CR maximums at the end of the acid injection phase at 0.17 h (Figure 5). The CR steadily increased with time of exposure thereafter, showing a very good reproducibility of results. As expected, a reduction in pH value led to enhanced film dissolution kinetics, as suggested by a more rapid CR increase. This result is in agreement with the findings of Crouch and Ryan on the localized dissolution of thin passive films on Fe-Cr alloys.[13] The final CRs in the low-pH experiments (e.g., pH 5.5) were not significantly lower than the ones for freshly prepared metal specimens immediately after immersion, suggesting that after dissolution the remaining films offered very little or no protectiveness.

Other "kinks" seen in the CR curves, different from the local peaks at the end of pH adjustment phase, stem from flow disturbances caused by the insertion and removal of various pieces of equipment (pH electrodes, sampling probes, syringes, etc.). Although this was necessary for process control and monitoring, even minor flow perturbations affected the measured CRs.

Measured Fe^{2+} concentration in bulk solution $[Fe^{2+}]_b$ for chosen pH values is shown in Figure 6. The increase in the concentration of ferrous ions tended to slow down with time, indicating a deceleration of the dissolution process. The reason for this is clear: as the dissolution of $FeCO_3$ proceeds, the concentration of Fe^{2+} and CO_3^{2-} in the bulk solution increases, leading to a spontaneous increase in pH value and a reduction in the driving force for dissolution.

Investigated SEM micrographs from these experiments show that the highest pH (pH 6.1) produced little visible damage. The cross-sectional and surface images (Figures 7[a] and 8[a]) show only a small number of open pores on the top film layer. In contrast, pH 5.8 led to significantly more damage, as shown in Figure 8(b), where quite a larger number of wider pores can be seen. Yet, the major difference has been observed with respect to the "inner" film layer where

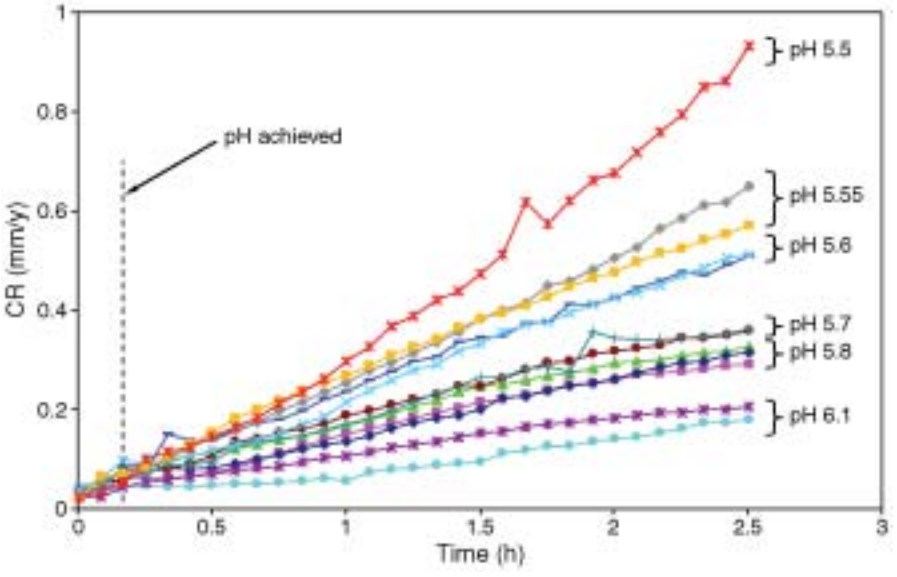

FIGURE 5. *CR increase during film dissolution at 10,000 rpm velocity in the pH 5.5 to 6.1 range.*

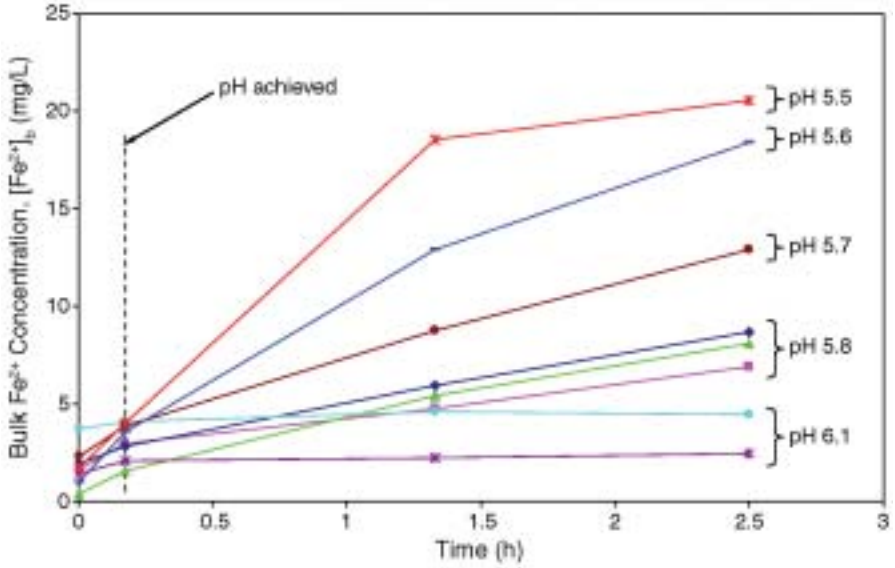

FIGURE 6. *Measured Fe^{2+} concentration in bulk solution $[Fe^{2+}]_b$ during film dissolution at 10,000 rpm velocity in the pH 5.5 to 6.1 range.*

a considerable dissolution of the film just beneath the top layer occurred (Figure 7[b]). This effect was nonuniform and indicates that film dissolution proceeds in a very selective way, i.e., that all $FeCO_3$ film grains are not "created equal" when it comes to dissolution. A further decrease in pH (pH 5.7) resulted in film morphology, shown in Figure 9(a), where some evidence of nonprogressed partial mechanical damage, i.e., microcracking along the dissolution weakened paths seems to appear. This damage, however, eventually progresses to bare, film-free areas at even lower pH values. Induced mechanical film removal from dissolution (mode M/D) at pH 5.5 is demonstrated in Figures 3(b) and 9(b).

The pH 5.8 was selected for further dissolution experimentation as it satisfied three requirements. First, it produced what was deemed "pure" dissolution damage (mode D), devoid of both M and M/D damage modes, confirming that studying film dissolution was possible without major interference from mechanical film removal mechanisms. Second, it was preferable to have slower dissolution kinetics to get the closest "match" with previously observed mechanical removal kinetics (in terms of magnitude). Third, it yielded films with clearly visible damage (in SEM) suitable for morphology assessment.

Effect of Velocity

To investigate the effect of velocity on dissolution, two series of experiments were conducted at pH 5.8: 10,000 rpm and 7,000 rpm. Each experiment was repeated three to five times. Figure 10 shows the CR increase for two velocities, while the corresponding measured $[Fe^{2+}]_b$ data plots are given in Figure 11. The resulting reproducibility of obtained results was very good. The local peaks in the CR curves, as well as periodically seen disturbances, have already been discussed in the preceding section. Clearly, higher velocity led to faster film dissolution kinetics. This seems to confirm the hypothesis that the transport of Fe^{2+}, originating from dissolved $FeCO_3$ film, from the surface-solution interface to bulk solution, is governed by convective diffusion as previously suggested.[5-6]

The SEM cross-sectional images of high- and low-velocity specimens are given in Figures 12 and 13, while the top-view ones are shown in Figures 14 and 15, respectively. A range of magnifications (from 100X to 1,000X) enabled more insight into the residual film structure. For the sake of clarity, the presented surface topography micrographs (Figures 14 and 15) were taken using the back-scattered electron (BSE) mode, as it emphasizes chemical compositional differences. This difference becomes more obvious by comparing Figures 14(b) and 8(b), which comprise basically the same image created using BSE and SE modes, respectively. Inspection of the cross sections seen in Figures 12 and 13 confirmed the pure chemical dissolution mechanism; however, different degrees of damage to the film were seen. High-velocity specimens exhibited more dissolution than low-velocity films, because the top film layer definitely had more damage. Another important piece of evidence is the difference in the inner film layer. The "black band" underneath the top layer appears wider at 10,000 rpm, suggesting a higher level of dissolution. Figures 14 and 15 corroborate the conclusions from the cross-sectional images, since the increased velocity resulted in a larger number of larger pores. It also should be noted that pores with an oblong shape were oriented in the streamwise direction.

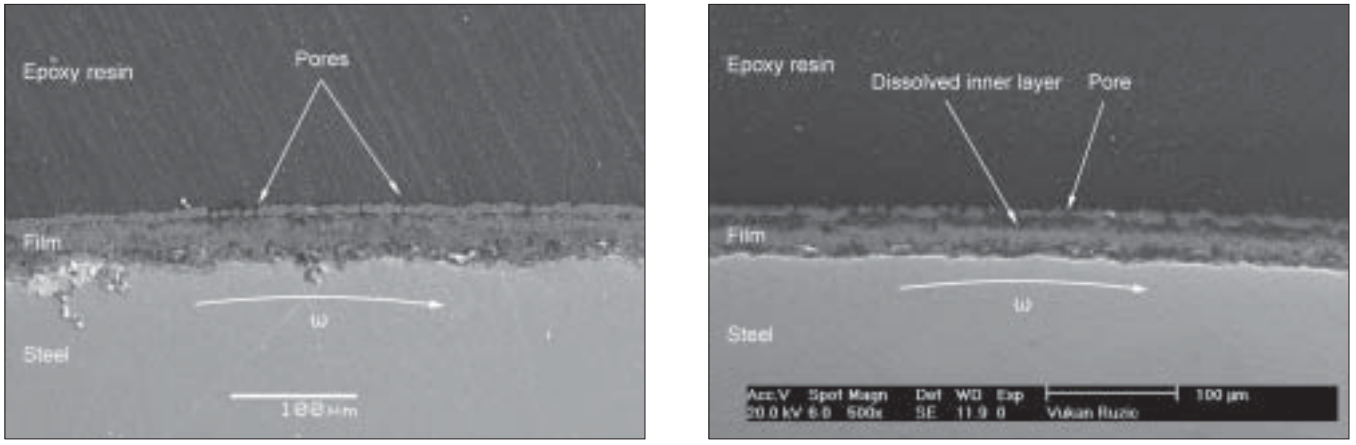

(a) (b)

FIGURE 7. *Typical cross section of $FeCO_3$ film at the end of the dissolution process at 10,000 rpm velocity and: (a) pH 6.1 and (b) pH 5.8 (mag. 500X).*

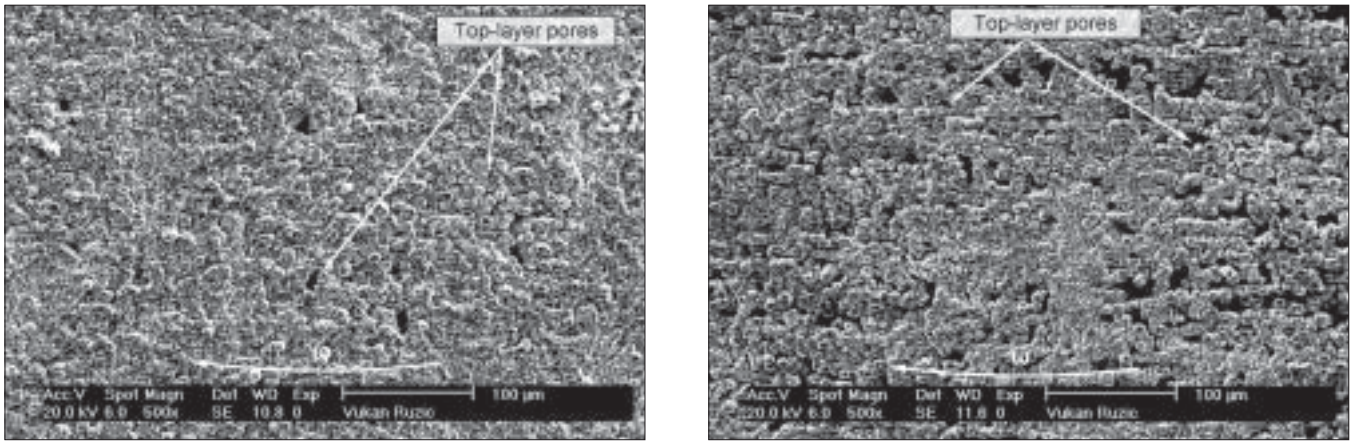

(a) (b)

FIGURE 8. *Typical surface topography of $FeCO_3$ film at the end of the dissolution process at 10,000 rpm velocity and: (a) pH 6.1 and (b) pH 5.8 (mag. 500X).*

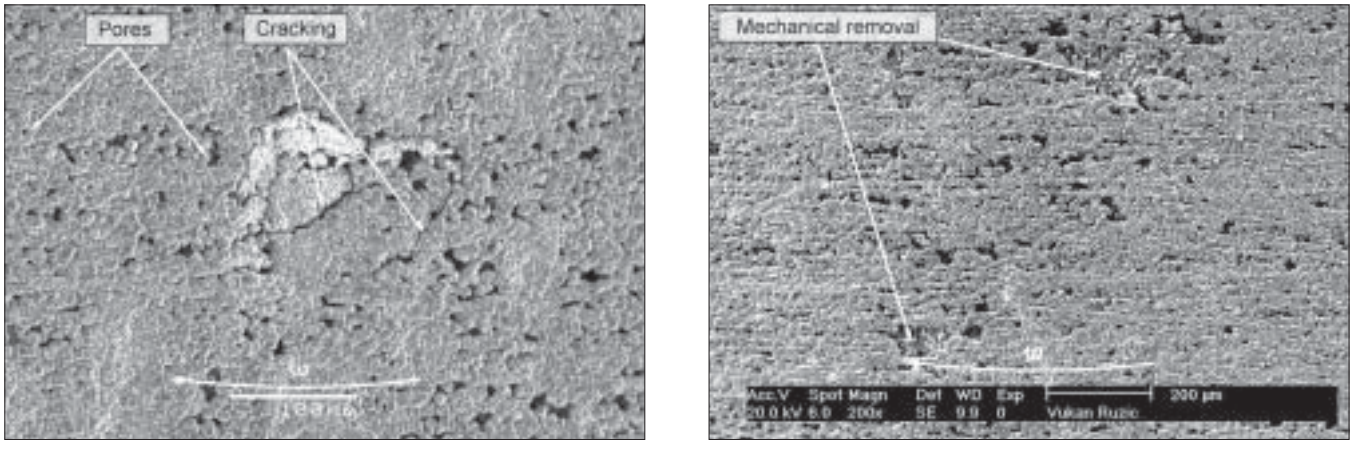

(a) (b)

FIGURE 9. *Surface topography of $FeCO_3$ film at the end of the dissolution process at 10,000 rpm velocity showing: (a) nonprogressed partial mechanical damage—cracking at pH 5.7 (mag. 500X) vs. (b) progressed mechanical damage—bare metal patches at pH 5.5 (Mag. 200X).*

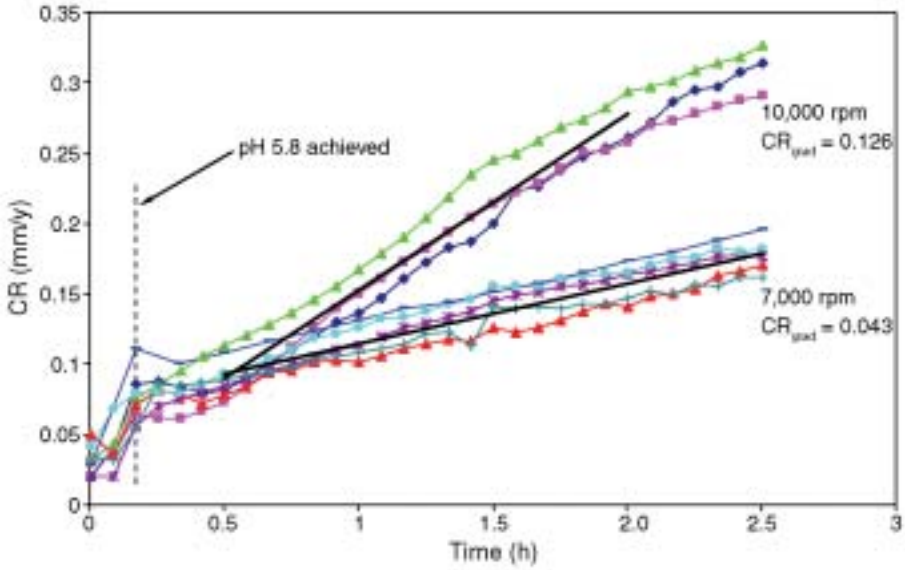

FIGURE 10. *CR increase during film dissolution at pH 5.8 for: 10,000 rpm and 7,000 rpm velocity.*

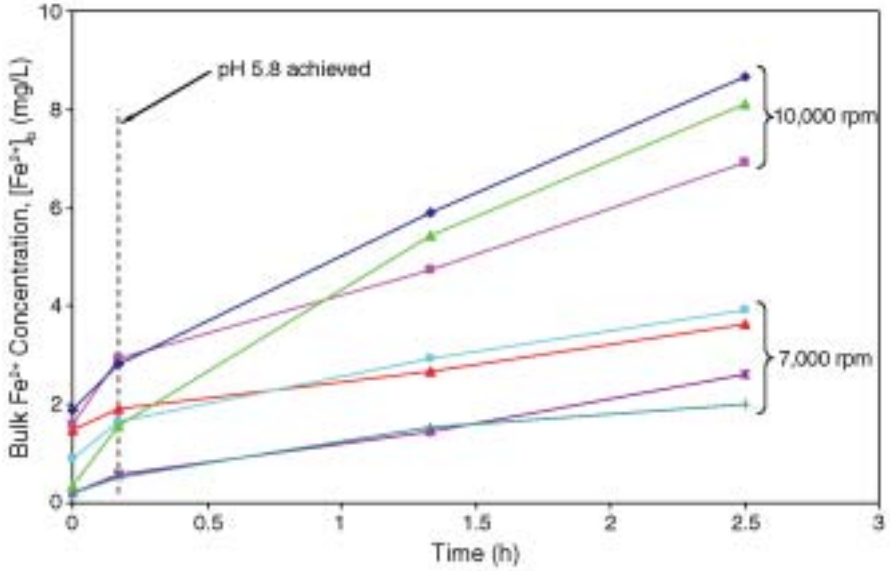

FIGURE 11. *Measured Fe^{2+} concentration in bulk solution $[Fe^{2+}]_b$ during film dissolution at pH 5.8 for: 10,000 rpm and 7,000 rpm velocity.*

DISCUSSION

Kinetics of Decoupled Mechanical and Chemical Film Removal

Pure chemical dissolution results are compared with some previously reported pure mechanical film removal results[3] for the same type of film (type B) and removal velocity (Figure 16). The CR gradient (CR_{grad}) was adopted as an indicator for comparison purposes because of the different time frames over which the two film removal experimental series were conducted. The dissolution appears to be far more detrimental to film integrity even at this relatively high pH value (pH 5.8). The ratio of dissolution to mechanical removal kinetics $(CR_{grad})_D/(CR_{grad})_M$ was 5.51 at lower velocities and it increased to 7.78 at higher velocities, suggesting a stronger dependence of the dissolution on velocity when compared to mechanical film removal.

In conclusion, the developed experimental procedures enabled the studies of evidently decoupled mechanical (mode M) and chemical dissolution (mode D) film removal mechanisms, making a comparison of the two viable even at the same velocity. This created a necessary foundation for the future investigation of the possible synergistic effect between them.

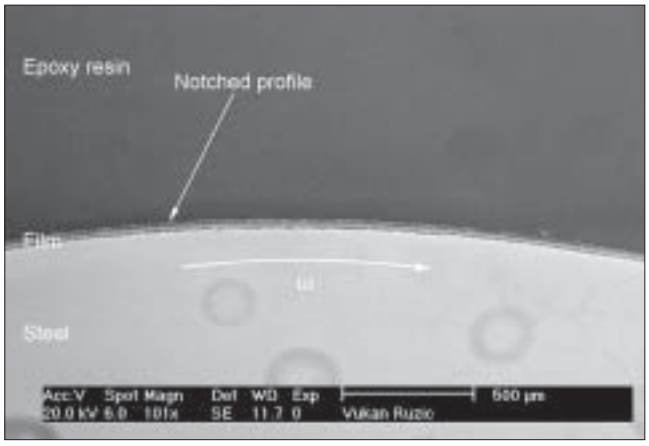

(a)

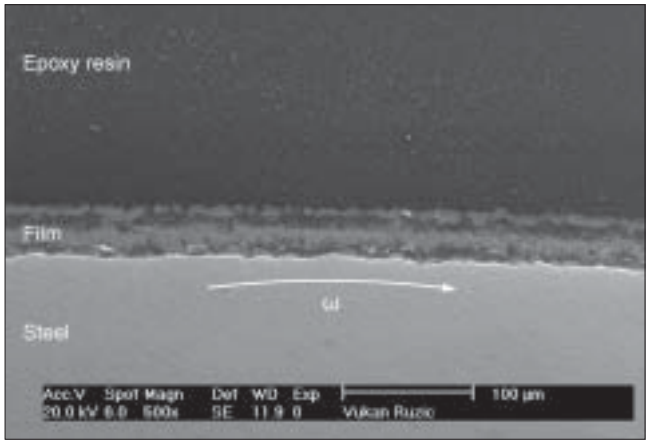

(b)

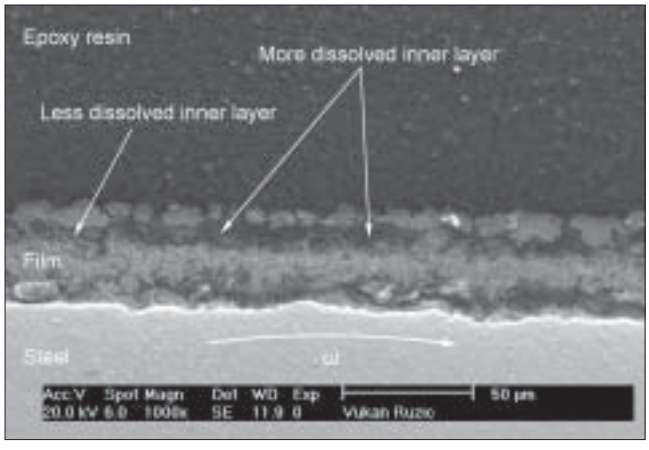

(c)

FIGURE 12. *Typical cross section of $FeCO_3$ film at the end of the dissolution process at 10,000 rpm velocity and pH 5.8 (mag.: [a] 100X, [b] 500X, and [c] 1,000X).*

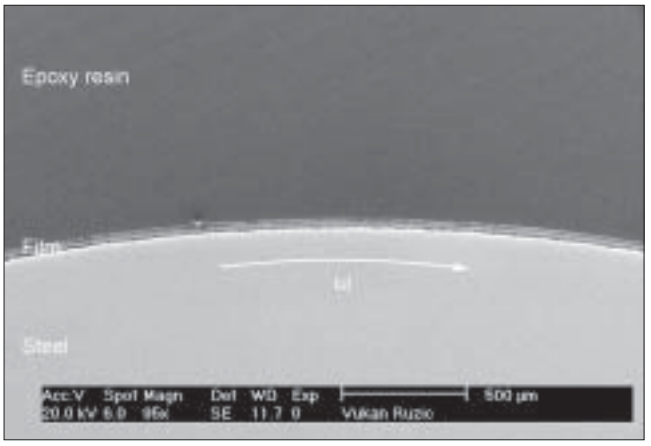

(a)

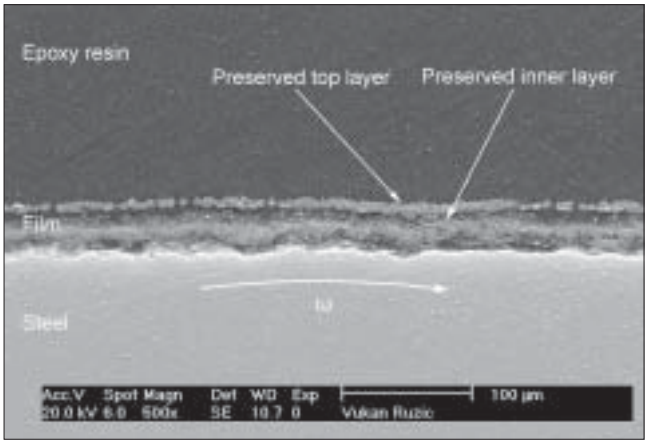

(b)

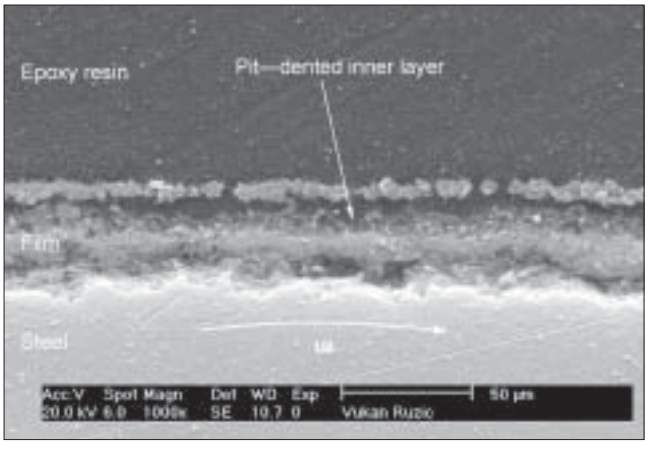

(c)

FIGURE 13. *Typical cross section of $FeCO_3$ film at the end of the dissolution process at 7,000 rpm velocity and pH 5.8 (mag.: [a] 100X, [b] 500X, and [c] 1,000X).*

Mechanism of Chemical Film Dissolution

Mass-Transfer-Controlled Dissolution Mechanism — Although the roles of chemical reaction and mass-transfer steps in the dissolution process are still debated in the open literature as to which is rate-determining,[9] it seems that prevailing opinion leans toward the mass transfer.[5-6] In the present study, this seems to be confirmed. While the film-dissolution kinetics dependence on pH can be explained both in terms of chemical and mass-transfer effects, the pro-

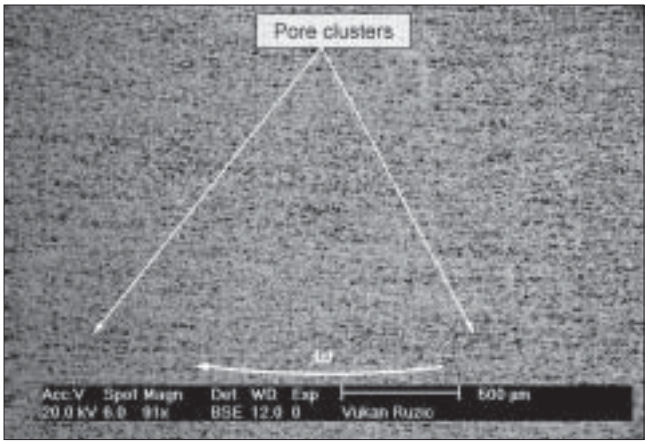

(a)

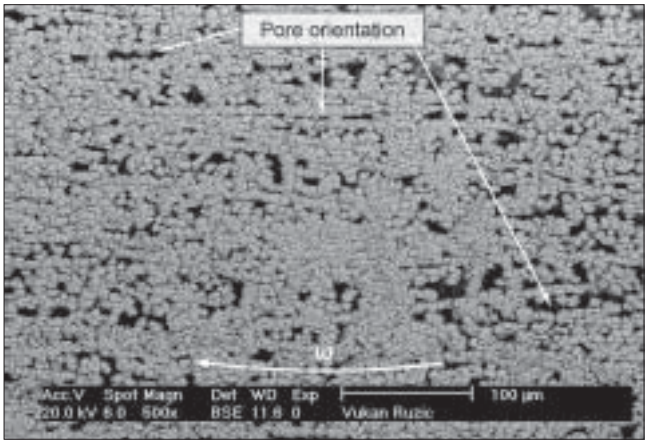

(b)

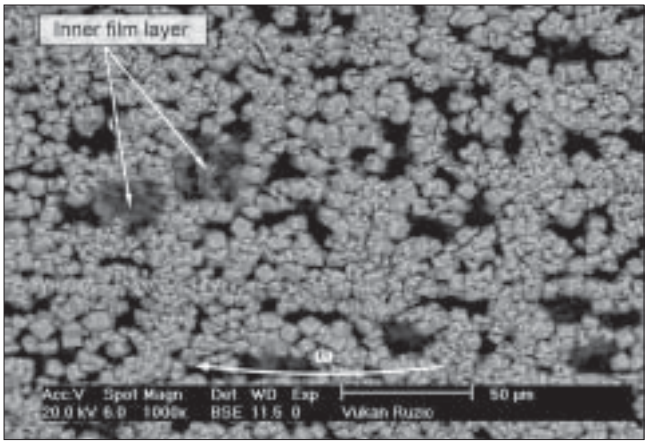

(c)

FIGURE 14. *Typical surface topography of $FeCO_3$ film at the end of the dissolution process at 10,000 rpm velocity and pH 5.8 (mag.: [a] 100X, [b] 500X, and [c] 1,000X).*

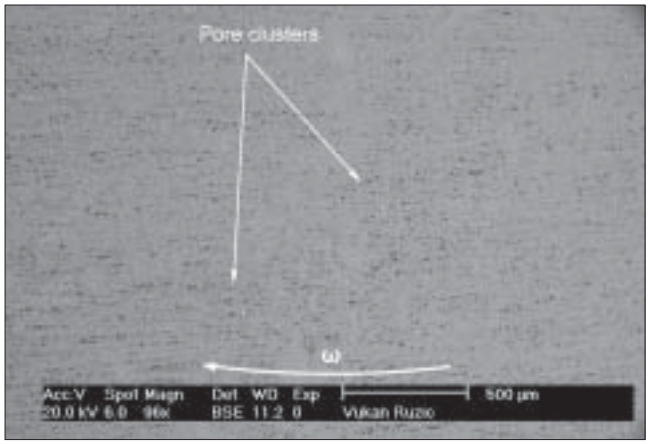

(a)

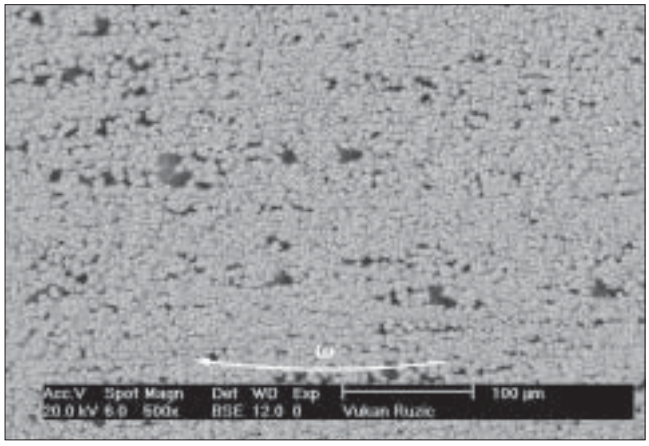

(b)

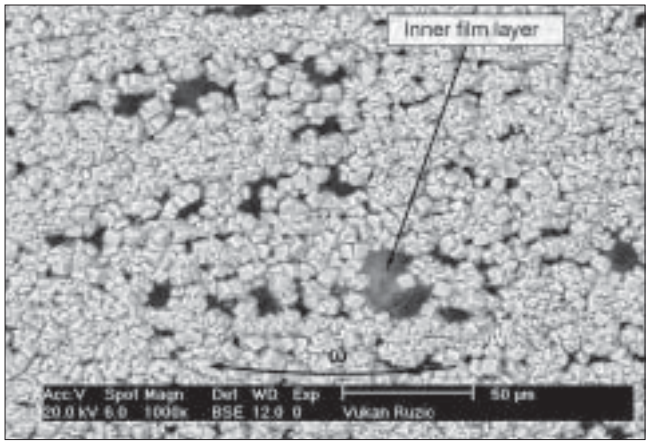

(c)

FIGURE 15. *Typical surface topography of $FeCO_3$ film at the end of the dissolution process at 7,000 rpm velocity and pH 5.8 (mag.: [a] 100X, [b] 500X, and [c] 1,000X).*

nounced effect of velocity seems to be clear proof of the mass-transfer dependence.

Following this conclusion, the rate of mass transfer, which at the same time represents the rate of film dissolution due to the mass transfer being the governing mechanism of $FeCO_3$ dissolution as well as the overall film removal rate for pure dissolution damage, i.e., mode D (pH ≥ 5.8), can be expressed as:

$$J = k_m([Fe^{2+}]_s - [Fe^{2+}]_b) \quad (3)$$

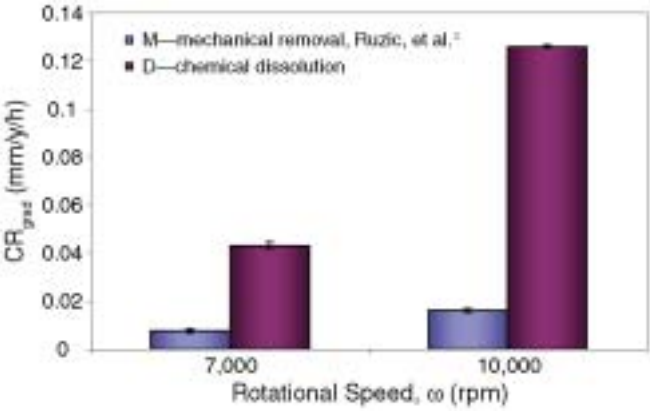

FIGURE 16. *Comparison of pure dissolution kinetics at pH 5.8 and pure mechanical film removal kinetics expressed via CR gradients at lower (7,000 rpm) and higher (10,000 rpm) velocities (bars represent standard deviation of the mean, i.e., standard error).*

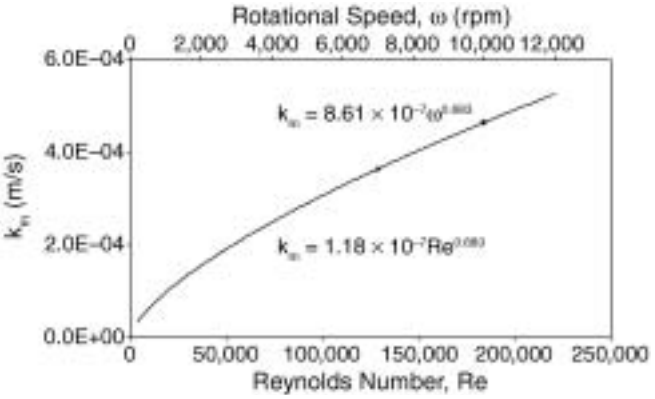

FIGURE 17. *Mass-transfer coefficient of Fe^{2+} species for the rotating cylinder geometry as a function of Reynolds number (rotational speed) at 80°C.*

where J is mass flux ($kg/m^2/s$), k_m is the mass-transfer coefficient (m/s), and $[Fe^{2+}]$ is the concentration of ferrous ions (kg/m^3) with subscripts s and b denoting surface and bulk conditions, respectively. The diffusion of Fe^{2+} species has to be the rate-limiting substep, since its diffusive capability is lower than that of CO_3^{2-} ions (0.72×10^{-9} vs. 0.92×10^{-9} m^2/s at 25°C, respectively).[15] For calculation purposes, the $[Fe^{2+}]_b$, which was directly measured, was assumed to originate from film dissolution only. It has been a reasonable assumption, since it was ascertained that the relative contribution of Fe^{2+} ions originating from the corrosion process (i.e., metal dissolution) had been many orders of magnitude smaller. The $[Fe^{2+}]_s$ was numerically computed by solving the system of all included chemical reactions for saturation condition, S = 1.

The k_m was obtained using the in-house empirical mass-transfer correlation determined for the utilized RC geometry:

$$Sh = 0.1012\,Re^{0.683}\,Sc^{0.356} \quad (4)$$

in which $Sh = k_m d/D$ (where d is the diameter of the cylindrical specimen in m and D is the diffusion coefficient in m^2/s), $Re = vd/\nu$ (where $v = \omega d/2$ is the peripheral velocity in m/s, ω is the angular speed in rad/s, and $\nu = 0.41 \times 10^{-6}$ m^2/s is the kinematic viscosity of the solution at 80°C obtained from Schmitt and Mueller[16]), and $Sc = \nu/D$ are Sherwood, Reynolds, and Schmidt numbers, respectively. The temperature correction for the diffusivity of iron-soluble species was taken into account by using the Stokes-Einstein empirical relationship:[17]

$$D = 2.5\times10^{-15}\,\frac{T}{\mu} \quad (5)$$

where T is absolute temperature (K) and $\mu = \nu\rho$ = dynamic viscosity (kg/m/s) with ρ being the density of the solution (ρ = 1,000 kg/m^3 at 80°C taken from Schmitt and Mueller[16]).

The resulting expression for the mass-transfer coefficient of the ferrous species at 80°C temperature as a function of Reynolds number is given by the following equation:

$$k_m = 1.18\times10^{-7}\,Re^{0.683} \quad (6)$$

The derived mass-transfer coefficient accounts for both the turbulent convection and molecular diffusion. The plot of k_m variation with Reynolds number and rotational speed with denoted velocities of interest is shown in Figure 17.

The increase in acid concentration in the solution was followed by a prompt and steep reduction in pH value during the pH adjustment phase. The targeted nadir was reached at 0.17 h. Beyond this point, pH tended to increase slightly until the end of the experiment due to the ongoing release of dissolution products (Fe^{2+} and CO_3^{2-}) into the bulk solution (Figure 18).

The plots of averaged measured Fe^{2+} concentrations in bulk solution $[Fe^{2+}]_b$ and corresponding calculated concentrations at the wall $[Fe^{2+}]_s$ for given pH and S = 1 are presented in Figures 19 and 20, respectively. As observed, the $[Fe^{2+}]_b$ experienced a sharp rise during the acid concentration increase and subsequent decelerating continual growth thereafter, as opposed to $[Fe^{2+}]_s$, which exhibited local peaks after an initial hasty increase followed by a less dramatic decline. Such $[Fe^{2+}]$ trends consequently produced a decline in concentration gradients $\Delta[Fe^{2+}] = [Fe^{2+}]_s - [Fe^{2+}]_b$ after the acid injection phase, which in turn slowed down mass-transfer (film dissolution) rates as demonstrated in Figure 21. In addition, Figure 21 points out the effect of velocity on mass transfer when comparing 10,000 rpm against the 7,000-rpm case at pH 5.8. A faster decrease in the mass-transfer rate

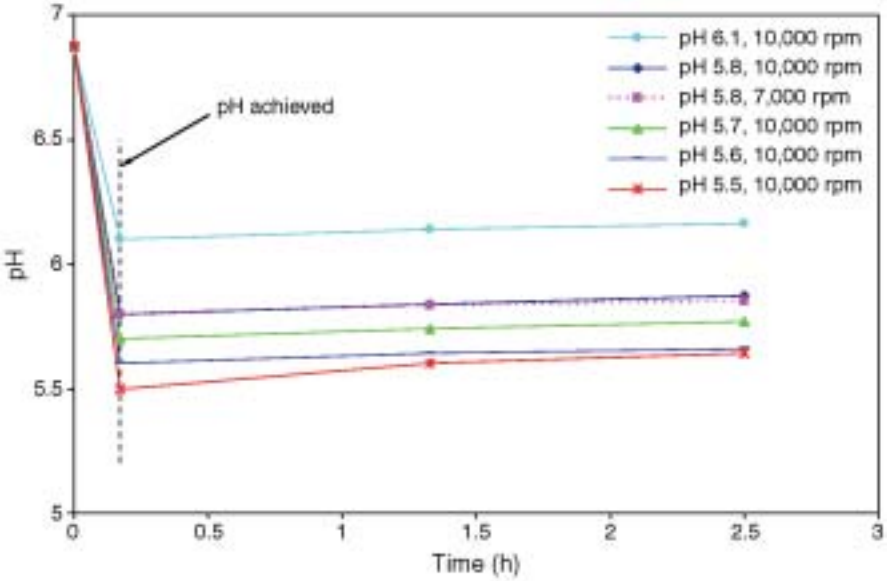

FIGURE 18. *Variation of mean measured pH with time during the film dissolution process.*

over time at 10,000 rpm was due to an overall faster dissolution kinetics at higher velocity that consequently led to a faster decrease in the concentration driving force, i.e., a faster dissolution attenuation. Unfortunately, owing to the limited number of data points, i.e., discrete mass-transfer rates, and even more so the fact that exact location of the actual local maximums and their corresponding values were unknown, it was not possible to appropriately determine the total (cumulative) mass transfer. Nevertheless, the superior dissolution kinetics at the higher velocity, which ultimately resulted in more dissolution damage, i.e., more $FeCO_3$ mass removed, is well evidenced both implicitly using the CR tool (Figure 10) and SEM techniques (Figures 12 through 15). The observed increase in the film removal kinetics with Reynolds number and acid concentration (pH decrease) agreed well with findings of Crocker, et al., who investigated the calcite scale dissolution.[8]

Selective Sequential Dissolution Mechanism — The visualized selective dissolution of the $FeCO_3$ may be explained by considering the morphology of the films prior to dissolution. Following the film formation procedure a two-layered film structure is obtained, and each layer seemed to be affected differently by the dissolution process. The top layer is a dense crystalline material primarily formed during the second stage of film formation, i.e., spontaneous film growth phase when relative supersaturation is low,[3] and therefore, when the particle growth mode, i.e., crystallization predominates.[18] In contrast, the more porous inner layer develops during the first, rapid precipitation stage of film formation at high supersaturations,[3] and hence, under these conditions, where the nucleation mode prevails, the film is formed by coagulation of crystal nuclei from a colloidal solution close to the metal surface.[18] Apparently, only limited crystallization occurs in the inner layer during the second stage. Therefore, the top film layer is a homogeneous, dense crystalline structure, while the inner film layer exhibits as a more porous and amorphous mixture of particulate and filamentary particles with pores only partially filled in with crystalline material. Consequently, a dense, more dissolution-resistant top film layer experiences only partial, nonuniform dissolution damage selectively augmented by erosion at weak spots. As a result, the randomly scattered pores emerge on the surface providing direct access to the more porous, dissolution-prone inner film layer that is affected by a severe uniform dissolution generally manifested as the layer-thinning effect. Besides being strongly pH- and velocity-sensitive, depending on these parameters, the dissolution process may easily induce a complementary mechanical removal mode (M/D) that would lead to the cracking and removal of significantly larger film patches (typically 100 microns and more, Figures 3[b] and 9) than under dissolution alone (less than 40 μm, Figures 14 and 15).

CONCLUSIONS

The chemical dissolution of $FeCO_3$ films in pH 3 to pH 6.1 and Re = 3.68×10^3 to 1.84×10^5 at 80°C using RC flow geometry has been studied. The main conclusions are:

❖ Pure chemical dissolution of protective corrosion $FeCO_3$ films in undisturbed, turbulent, single-phase flow seems to be mass-transfer-controlled as suggested by a strong correlation found between velocity and film removal kinetics implicitly monitored via CR.

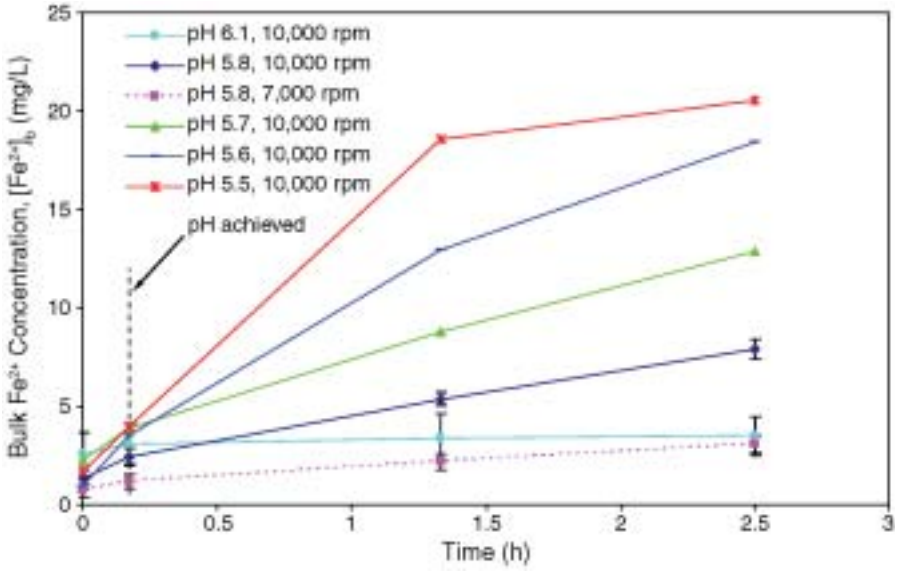

FIGURE 19. *Mean measured Fe^{2+} concentration in bulk solution during the film dissolution in the pH 5.5 to 6.1 range (bars represent standard deviation of the mean, i.e., standard error).*

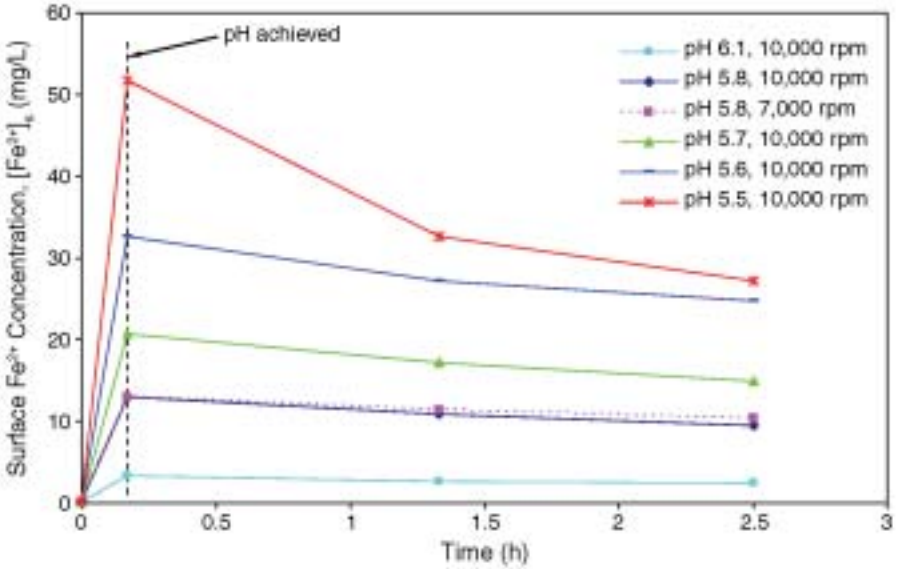

FIGURE 20. *Predicted Fe^{2+} concentration at the film-solution interface during the film dissolution process calculated for saturated condition (S = 1) given the measured pH.*

❖ Film dissolution removal kinetics and the severity of film damage are strongly dependent on the pH value, i.e., the level of undersaturation in the solution.
❖ The controlled, pure dissolution mechanism leads to only partial and selective film removal with lots of open pores on a more dissolution-resistant crystalline top film layer, which further exposes a more porous, dissolution-susceptible inner layer to a severe and uniform "undermining" dissolution.

Further study has been undertaken with the goal of reaching a conclusive answer as to whether there is a synergistic effect due to the simultaneous action of mechanical and chemical film removal in single-phase turbulent flow. These results will be reported in a separate paper.

ACKNOWLEDGMENTS

The authors acknowledge the financial support provided by the Australian Government in the form of an Australian Postgraduate Award Scholarship held by V. Ruzic.

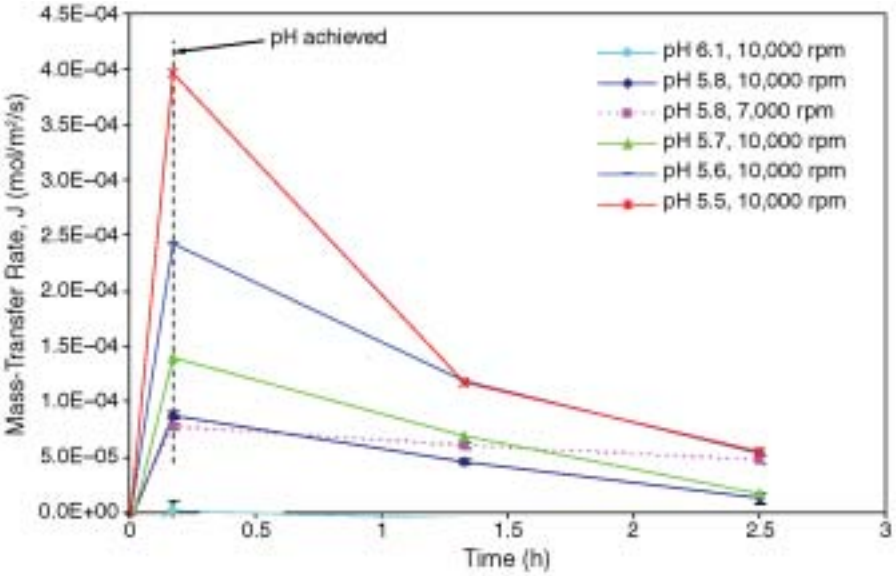

FIGURE 21. *Variation of mass-transfer (dissolution) rates during the film dissolution process (bars represent standard deviation of the mean).*

REFERENCES

1. J.-L. Crolet, "Protectiveness of Corrosion Layers," in Modelling Aqueous Corrosion: From Individual Pits to System Management, Proc. NATO Advanced Research Workshop, NATO ASI Series, Series E, Applied Sciences: no. 266, eds. K.R. Threthewey, P.R. Roberge, held Sept. 6-8, 1993 (Dordrecht, The Netherlands: Kluwer Academic Publishers, 1994), p. 1.
2. F.D. de Moraes, J.R. Shadley, J. Chen, E.F. Rybicki, "Characterization of CO_2 Corrosion Product Scales Related to Environmental Conditions," CORROSION/2000, paper no. 30 (Houston, TX: NACE International, 2000).
3. V. Ruzic, M. Veidt, S. Nešić, Corrosion 62, 5 (2006): p. 419.
4. S. Nešić, J. Postlethwaite, S. Olsen, Corrosion 52, 4 (1996): p. 285.
5. B.S. Poulson, "Erosion Corrosion," in Corrosion, eds. R.A. Jarman, G.T. Burstein, L.L. Shreir, vol. 2, 3rd ed. (Oxford, U.K.: Butterworth-Heinemann, 1994), p. 1:293.
6. A. Dugstad, "The Importance of $FeCO_3$ Supersaturation on the CO_2 Corrosion of Carbon Steels," CORROSION/92, paper no. 14 (Houston, TX: NACE, 1992).
7. K. Videm, A. Dugstad, Mater. Perform. 28, 3 (1989): p. 63.
8. M.R. Crocker, P.G. Fairhurst, D.I. Wilson, "Model Experiments of Crystalline Scale Removal," The 1996 IChemE Research Event—Second European Conference for Young Researchers in Chemical Engineering, held April 2-3 (Leeds, U.K.: IChemE, 1996), p. 853.
9. C.J. Wilson, P.R. Lockyer, D.I. Wilson, "Modelling of Crystalline Scale Removal," Proc. Int. Conf. Mitigation of Heat Exchanger Fouling and Its Economic and Environmental Implications, ed. T.R. Bott, held July, 1999 (Banff, Alberta: Begel House, Inc., 1999), p. 314.
10. C.J. Boxley, H.S. White, J. Electrochem. Soc. 151, 5 (2004): p. B265.
11. S. Wolynec, D.R. Gabe, Corros. Sci. 12 (1972): p. 437.
12. F. Giralt, O. Trass, Can. J. Chem. Eng. 54 (1976): p. 148.
13. D.S. Crouch, M.P. Ryan, Corros. Mater. 29, 6 (2004): p. S1.
14. D.C. Silverman, Corrosion 40, 5 (1984): p. 221.
15. J. Kvarekval, "A Kinetic Model for Calculating Concentration Profiles and Fluxes of CO_2-Related Species Across the Nernst Diffusion Layer," CORROSION/97, paper no. 5 (Houston, TX: NACE, 1997).
16. G. Schmitt, M. Mueller, "Critical Wall Shear Stress in CO_2 Corrosion of Carbon Steel," CORROSION/99, paper no. 44 (Houston, TX: NACE, 1999).
17. B. Chexal, J. Horowitz, B. Dooley, P. Millett, C. Wood, R. Jones, M. Bouchacourt, F. Remy, F. Nordmann, P. Saint Paul, W. Kastner, "Flow-Accelerated Corrosion in Power Plants," Joint Electric Power Research Institute, Inc., Electricite de France and Siemens AG Power Generation Report, TR-106611-R1, July, 1998.
18. A. Dugstad, "Mechanism of Protective Film Formation During CO_2 Corrosion of Carbon Steel," CORROSION/98, paper no. 31 (Houston, TX: NACE, 1998).